


RESEARCH

Open Access



Arterial spin-labeled magnetic resonance perfusion imaging in prediction of pediatric brain tumors grading: inter-observer agreement

Maha Mohammed Hassan Elmansy^{1*} , Samia Mounir Zaki¹, Magda Ali Hany Elbakry¹ and Rihame Mohamed Abdelwahab¹

Abstract

Background Pediatric brain tumors are a major concern with many variable management options. Arterial spin-labeled magnetic resonance perfusion imaging is a relatively new and noninvasive technique that can help in predicting tumor grades and provide us with physiological data about the tumors which significantly aids in all stages of tumor care, including diagnosis, therapy, and follow-up.

Aim of the study To determine agreement between independent observers in the assessment and prediction of brain tumor grading in pediatrics by arterial spin-labeled (ASL) magnetic resonance perfusion imaging.

Methods Thirty-two patients (21 boys and 11 girls; mean age of (10.28 ± 4.31) years) with brain tumors were evaluated by ASL MRI perfusion. Image analysis was performed by two reviewers for quantifying absolute and relative tumoral blood flow (aTBF and rTBF) as well as qualitative assessment of the tumors in ASL color map images.

Results The inter-observer agreement for the mean aTBF and the mean rTBF values of the studied lesions was almost perfect (inter-class correlation coefficient (ICC) = 0.978, 0.997). There was substantial agreement between both observers for the qualitative assessment of the studied lesions in color ASL images (Kappa = 0.779, with % of agreement = 87.0%). The mean aTBF for grade I tumors was (24.64 ± 3.45) ml/100 g/min, for grade II tumors it was (33.81 ± 3.59) ml/100 g/min, while for high-grade tumors (grade III and IV tumors) it was (75.60 ± 20.0) ml/100 g/min with ($p < 0.001$). The mean rTBF of grade I, II, and III/IV tumors was (1.01 ± 0.17) ; (1.07 ± 0.31) ; and (3.12 ± 0.24) with ($p < 0.001$).

Conclusions Arterial spin-labeled perfusion MRI can help in the challenge of prediction of brain tumor grading in pediatrics with accurate quantitative and semi-quantitative measurements of perfusion parameters of the tumors as well as qualitative and visual assessment of the tumors.

Keywords Brain tumors, Arterial spin labeling, Pediatrics, Perfusion, MRI

Background

Central nervous system (CNS) tumors are one of the most common pediatric solid tumors with a high rate of cancer-related morbidity and mortality in childhood. Its incidence differs by age, sex, geography, and race [1, 2].

Pediatric CNS tumors are widely variable and different from adults in their signs, symptoms, location, and long-term sequelae, which sometimes cause delayed diagnosis and more difficult surgical resection. Therefore they need

*Correspondence:

Maha Mohammed Hassan Elmansy
maha.mansy@yahoo.com

¹ The Department of Diagnostic and Interventional Radiology, Faculty of Medicine, Mansoura University, Mansoura, Egypt

accurate preoperative assessment and a specialized multidisciplinary team [3–5].

The clinical presentation of pediatric brain tumors is also widely variable and affected by the patient's age, tumor location, effect on adjacent structures, and pattern of growth. They may be presented by focal symptoms, symptoms of increased intracranial pressure, or hydrocephalus. Infants may also be presented with failure to thrive [6–8].

In this context, imaging has a vital role in preoperative diagnosis and planning of those cases. Computed tomography has a limited diagnostic value and is not preferred in pediatrics because of radiation exposure, so it should be used only in emergencies or if MRI is not available [9, 10]. For the diagnosis of pediatric brain tumors, MRI is the gold standard method. Although conventional MRI sequences are useful in the detection of brain tumors in children, they frequently lack the sensitivity and specificity for determining the histopathological type of the tumor as there is a wide range of histopathological features included in pediatric brain tumors. Special MRI sequences such as functional MRI, perfusion-weighted images, and diffusion-weighted images help in determining the tumor type and grade [11, 12].

Arterial spin labeling is a method for measuring tissue perfusion using magnetic resonance imaging which is rapid, noninvasive, and applicable in routine brain MRI imaging [13–15]. It allows the quantification of tissue perfusion by the use of flowing arterial blood as a freely diffusible tracer. It uses radiofrequency pulses to alter the longitudinal magnetization of the blood before it reaches the region of interest to obtain a label image, and then it is repeated without magnetization of the blood to obtain the control image, and finally subtracting both images provides us with the ASL perfusion-weighted images [16–18].

The aim of our work was to highlight the role of the clinical application of ASL perfusion MRI in the grading of pediatric brain tumors as they have variable pathological features, which cause diagnostic challenges. Our study was based on agreement between independent observers and correlation with histopathological findings in order to determine the role of ASL perfusion study in the prediction of brain tumor grading in children. Therefore, better planning and management for those patients would be available.

Methods

Patients

The study was approved by the institutional review board of our institution, and informed verbal consent was obtained from the patient's parents. A prospective study was conducted on 35 consecutive children

who were referred from the neurosurgery department and outpatient clinic in the duration between December 2020 and December 2022. The inclusion criteria were: (1) patients with a pathologically proven or provisionally diagnosed to have a brain tumor, (2) patients with a known history of previous excision of a brain tumor and proven or provisionally diagnosed to have a recurrent brain tumor, and (3) patients 18 years old or younger of both genders were included. We excluded 3 patients from the study (2 cases showed marked motion artifacts and one case proved to be an abscess). The final patients enrolled in our study were 32 children (11 girls and 21 boys). Their ages range from 1 to 17 years. All patients were subjected to a clinical neurological examination and underwent MRI.

MRI technique

The technique was performed using a 1.5 Tesla MRI scanner (Ingenia, Philips). All patients were examined in the supine position using a head and neck coil, with the head maintained in a neutral position. Non-cooperative patients (7 patients) were subjected to sedation by oral chloral hydrate syrup at a dose of 50–75 mg per kilogram (mg/kg), with a maximum dose of 2000 mg. Those patients were fasting for 3–6 h before the examination because of the sedation's potential aspiration risk.

The planes obtained were axial, sagittal, and coronal. The sequences obtained were: T1-weighted images (T1WIs), T2-weighted images (T2WIs), fluid-attenuated inversion recovery (FLAIR), post-intravenous (IV) contrast T1WI study (gadoterate meglumine was administered at a dose of 0.5 ml per kilogram (ml/kg) body weight with a maximum dose of 10 ml at a flow rate of about 2 ml/s using a 20- to 22-gauge venous cannula) as an intravenous bolus injection at a flow rate of approximately 2 ml/s except in two cases (a 16-year-old pregnant female and a 4-year-old boy with poor renal function), diffusion-weighted images (DWI), and ASL perfusion MRI imaging.

The sequences parameters were: T1WI: repetition time (TR)=600 ms (ms), echo time (TE)=25ms, T2WI: TR=6000 ms, TE=90 ms, FLAIR: TR=10,000 ms, TE=115 ms, TI=2700 ms, matrix 80×80, field of view (FOV)=250×170 mm (mm), and slice thickness=5 mm.

Diffusion-weighted images were done in the axial plane before contrast medium administration by using a single-shot echo-planar imaging sequence. The following parameters were used: TR=5000 ms, TE=80 ms, inter-slice gap=1 mm, slice thickness=6 mm, and FOV=240×240 mm. Lesions of interest were scanned using the b values: zero, 500, and 1000 s/mm².

ASL data acquisition

Arterial spin-labeled perfusion imaging was carried out with a pseudo-continuous labeling technique. Following the labeling pulse, numerous time points were obtained. Fast spin echo single-shot echo planner imaging parallel sequences, maximum water fat shift, and a short TE to keep a good signal to noise ratio. The following parameters were used: a 1.5 mm inter-slice gap, 6 slices with an axial slice thickness of 6 mm, Voxel size was $3.6 \times 3.5 \times 3$ mm, field of view (FOV) was 240×240 mm, data matrix was 68×68 , TR/TE was 250/20, and the entire scan duration was four minutes.

Image analysis

Conventional MR images were reviewed for the detection of space occupying lesions (SOLs) and the primary characterization of detected lesions. The SOLs were reviewed for their site, size, consistency, signal intensity, contrast enhancement, and associated mass effect and edema. Automatically generated apparent diffusion coefficient (ADC) maps were generated and interpreted with correlation with DWIs to classify lesions into free or restricted diffusion.

Post-processing

The vendor's provided workstation (extended MR Workspace 2.6.3.5, Philips Medical Systems Nederland B.V.) was used to transfer the DICOM pictures. Subtraction of alternating tag and control image pairs, motion correction, and development of an ASL grayscale and colored map were the steps used in the post-processing of arterial spin-tagging data. Regions of interest (ROIs) were manually placed within the high signal area on the ASL grayscale map. The size of ROIs in both regions was similar to each other (ranging from 0.25 to 2.0 cm²). Compared to other conventional MR images, areas of arteries, calcification, hemorrhage, cysts, and necrosis were avoided.

Quantitative absolute TBF analysis

To quantify absolute TBF values, the following equation must be solved [19]:

$$CBF = \frac{\Delta M(TI_2)}{2M_{0,blood} \alpha TI_1 q_p (T_{1,tissue}, T_{1,blood}, TI_2)} e^{\left(\frac{TI_2}{T_{1,blood}}\right)} \quad (1)$$

where CBF stands for cerebral blood flow, $M(TI_2)$ for the mean signal intensity difference between label and control images, $M_{0,blood}$ for the equilibrium magnetization of blood, is the tagging efficiency, TI_1 for the duration of the tagging bolus, TI_2 for each slice's inversion time, T_1 , blood for the longitudinal relaxation of blood, and qp for

a correction factor that takes into account the difference between the T_1 of blood and the T_1 of brain tissue. The T_1 of the tissue is one of many variables that are directly measured before being added to the equation. Standard values from the published literature are represented by other variables in the equation. Although it would be ideal to gather each patient's variables de novo, this is not always feasible or practical, and the quantification may contain mistakes as a result of these assumptions. The T_1 levels of the blood and tissue are the most important values. Interpretations of the quantified CBF readings will be more accurate if you are aware of the influences and factors in the CBF quantification equation.

Semi-quantitative relative TBF analysis

A region of interest (ROI) was placed over the tumor region as in quantitative analysis, and another ROI was placed over the contralateral normal-appearing gray matter. Then the value of tumor ROI was divided by the value of ROI in the contralateral normal gray matter to estimate relative tumoral blood flow (rTBF) values.

Qualitative analysis of ASL color-coded maps

Color-coded ASL maps were visually analyzed by both observers, and the tumor region's perfusion was classified into 3 main categories: hyper-perfusion, hypo-perfusion, and mixed perfusion according to the color scale.

Statistical analysis and data interpretation

The images were reviewed by two radiologists (RA 16 years of experience, ME 9 years of experience in diagnostic radiology) who independently reviewed the images. Each reader was blinded to the results of the other reader. The data were then fed to the computer and analyzed using IBM SPSS Corp., Released in 2013. IBM SPSS Statistics for Windows, version 22.0 Armonk, NY: IBM Corp. Qualitative data were described using numbers and percentages. Quantitative data were described using the mean and standard deviation for normally distributed data. The significance of the obtained results was evaluated at the (≤ 0.05) level. Additionally, Chi-square and Fischer exact tests were used to compare qualitative data between groups as appropriate.

Receiver operating characteristic (ROC) curve analysis was used for evaluation of validity and cutoff point in comparison with ensured diagnostic test. Sensitivity and Specificity were detected from the curve, and positive predictive value (PPV), negative predictive value (NPV), and accuracy were calculated through cross-tabulation.

For the determination of the agreement, we investigated;

- Bland altman analysis and inter-class correlation for continuous variables
- Kappa agreement was calculated by cross-tabulation for categorical variables with Kappa

Kappa < 0: No agreement

Kappa between 0.00 and 0.20: Slight agreement

Kappa between 0.21 and 0.40: Fair agreement

Kappa between 0.41 and 0.60: Moderate agreement

Kappa between 0.61 and 0.80: Substantial agreement

Kappa between 0.81 and 1.00: Almost perfect agreement.

Results

Baseline characteristics

This study included 32 patients, 21 boys (65.6%) and 11 girls (34.4%), whose ages ranged from 1 to 17 years, and the mean age was (10.28 ± 4.31) years. The main clinical symptoms of the patients who were enrolled in this study were headache, nausea, vomiting, dizziness, seizures, educational or behavioral problems, and visual difficulties. The patients were grouped according to pathological findings into low-grade tumors (WHO grade I and II) including 23 patients (craniohypopharyngioma (4) (Fig. 1), meningioma (2), low-grade glioma (2), pilocytic astrocytoma (8) (Fig. 2), choroid plexus papilloma (2), dysembryoplastic neuroepithelial tumor (2), pineal body tumors (2) (Fig. 3), and PXA (1)) and high-grade tumors (WHO grade III and IV) including 9 patients (high-grade glioma (5) (Fig. 4) and medulloblastoma (4) (Fig. 5).

Conventional MRI features of studied lesions were analyzed regarding tumors' consistency (solid (20), cystic with solid nodule (8), and partially cystic partially solid (4) lesions), Contrast enhancement; (Non enhancing (2), heterogeneously enhancing (14), homogeneously enhancing (7), and cyst with enhancing mural nodule (7) lesions) and diffusion restriction (free diffusion (18) and restricted diffusions (14)). We classified the studied lesions according to the site of the lesion into cerebral hemispheres (8), posterior fossa (12), sellar/suprasellar (4), intraventricular (2), pineal (2), and brain stem/thalamus (4) (Table 1).

Absolute and relative tumoral blood flow

The mean absolute tumoral blood flow (aTBF) of the studied lesions was 28.9 (18.45–103.52) ml/100 g/min as measured by the first observer and 28.45 (3.51–102.88) ml/100 g/min by the second observer. The mean relative tumoral blood flow (rTBF) of the studied lesions was 1.01 (0.81–3.56) by the first observer and 1.11 (0.85–3.42) by

the second observer. There was excellent inter-observer agreement as regards both the mean aTBF (Fig. 6) and rTBF (Fig. 7), with the inter-class correlation coefficient (ICC) (95% CI) being 0.978 for the aTBF and 0.997 for the rTBF (Table 2).

Qualitative assessment

Regarding the qualitative assessment of the studied lesion in both gray and color ASL maps, the lesions were classified by both observers into hypo-perfused ($n=20$, 18), hyper-perfused ($n=7$, 7), and mixed perfusion ($n=5$, 7). There was substantial agreement between both observers (Kappa=0.779), with a percentage of agreement of 87.0% (Table 3).

Tumor grading

According to the 2021 WHO Classification of Tumors of the Central Nervous System, we classified the studied lesions into low-grade (WHO grades 1 and 2) and high-grade (WHO grades 3 and 4) tumors. Both absolute and relative TBF were significantly higher in high-grade tumors than in low-grade tumors. The mean aTBF for grade I, II, and III/IV tumors was (24.64 ± 3.45) ml/100g/min, (33.81 ± 3.59) ml/100 g/min, and (75.60 ± 20.0) ml/100 g/min. The mean rTBF for grade I, II, and III/IV tumors was (1.01 ± 0.17) , (1.07 ± 0.31) , and (3.12 ± 0.24) . There was a good correlation between calculated absolute and relative TBF and the WHO grades of the tumors with ($P < 0.001$) (Table 4).

ROC curve analysis

On the ROC curve, the area under curve (AUC) for aTBF and rTBF of the tumors to differentiate low-grade (grades I/II) from high-grade (III/IV) tumors was (0.979 and 0.969). Selection of (54.29 ml/100 g/min) and (2.84) as cutoff points of aTBF and rTBF of the tumoral regions to differentiate between low- and high-grade tumors revealed an accuracy of (93.8%), sensitivity of (87.5%), specificity of (95.8%), PPV of (87.5%), and NPV of (95.8%) (Fig. 8) (Table 5).

Discussion

Preoperative radiological assessment and accurate diagnosis and grading of brain tumors are very important in guiding therapeutic decisions. The strategy of treatment varies widely according to the type, location, and grade of the tumor. Although histopathologic evaluation is believed to be the gold standard tool in the diagnosis and grading of brain tumors, it has many limitations, such as its dependence on invasive biopsies or surgical removal of a tumor, sampling errors, and inaccurate grading caused by the heterogeneity of the tumors due to internal necrotic components [20, 21].

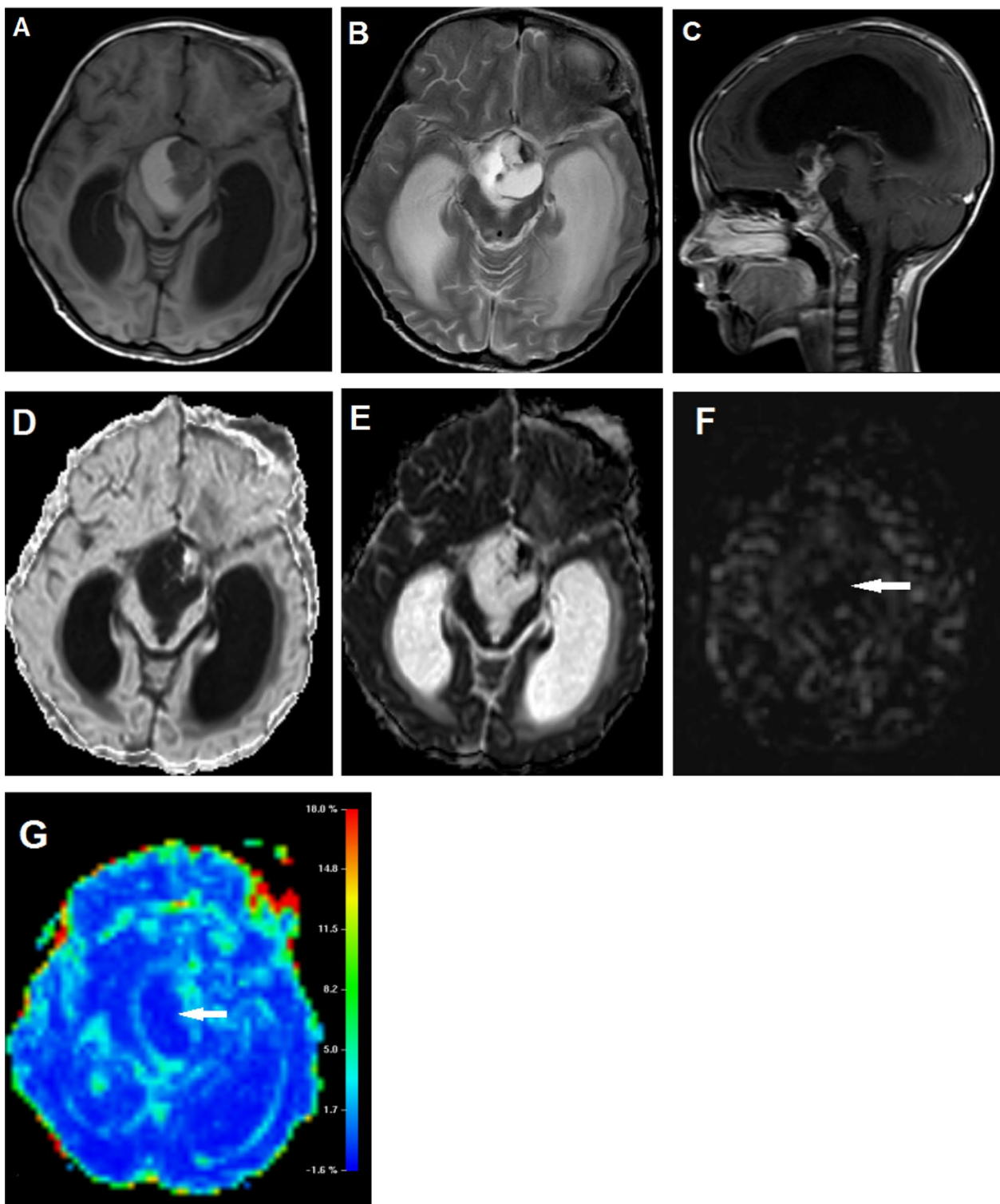


Fig. 1 A 6-year-old boy patient with a WHO grade I adamantinomatous craniopharyngioma. Images show a well-defined partially cystic, partially solid supra-sellar mass complicated by supratentorial hydrocephalic changes. The cystic parts display high signal intensity on axial T1WI (A) and mixed high signal intensities on axial T2WI (B) denoting a high proteinaceous content. The solid parts show strong enhancement on post contrast sagittal T1WI (C). Free diffusion of the lesion is seen in the form of low SI on DWI (b1000 image) and high SI on axial ADC grayscale map (D, E). Hypo-perfusion of the lesion (white arrows) is demonstrated in the axial ASL grayscale and color CBF maps (F, G)

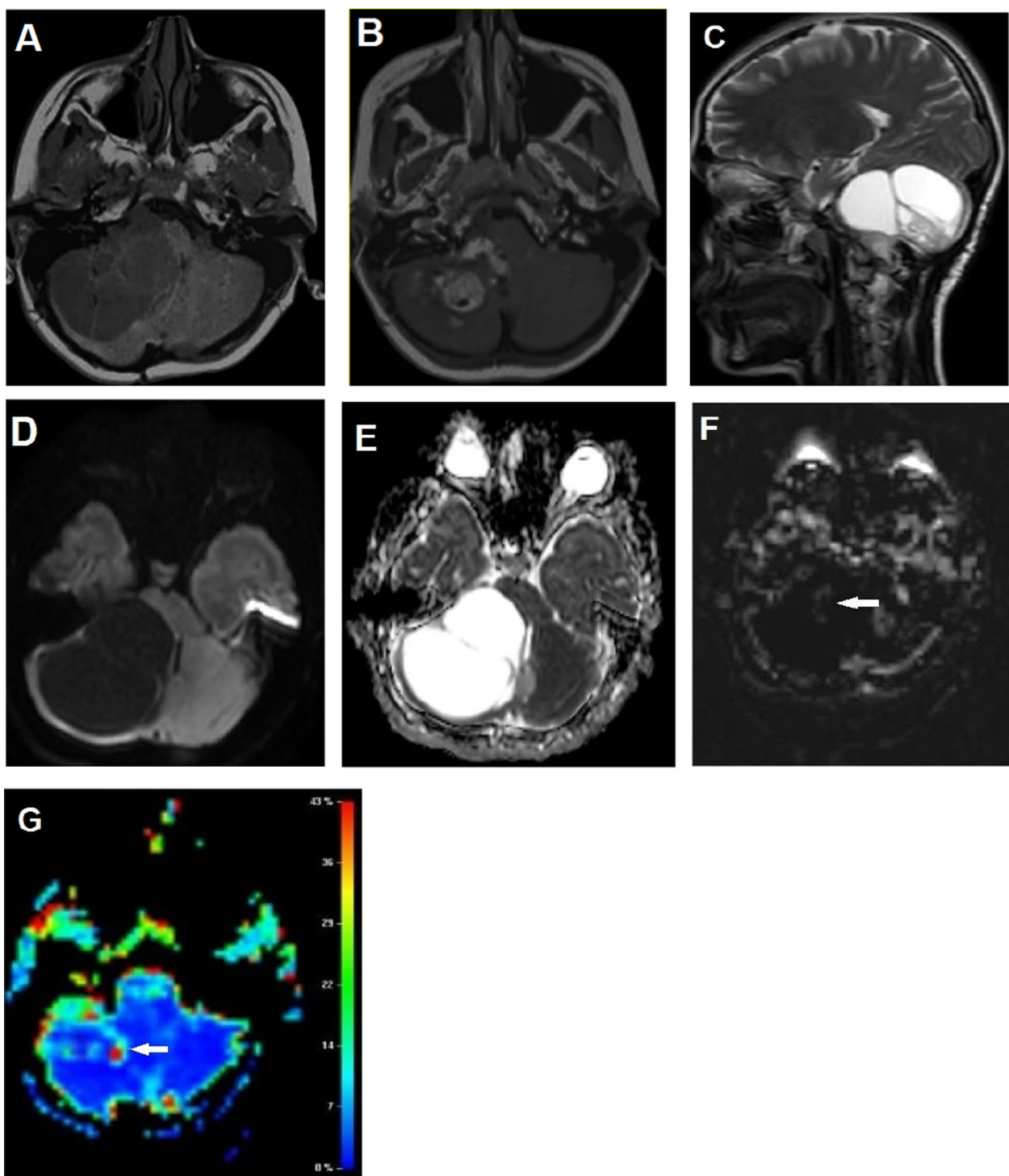


Fig. 2 A 14-year-old girl patient with a WHO grade I pilocytic astrocytoma. Images show a well-defined cystic lesion in the right cerebellar hemisphere with internal septae and solid mural nodule. It displays low signal intensity on axial T1WI (**A**) with enhancing mural nodule on post contrast axial T1WI image (**B**). It displays high SI of the cystic part with intermediate SI of the mural nodule on sagittal T2WI (**C**). Free diffusion of the lesion is seen in the form of low SI on DWI (b1000 image) and high SI on axial ADC grayscale map (**D, E**). Hypo-perfusion of the cystic parts with small area of hyper-perfusion (white arrows) corresponding to the solid mural nodule is seen in the axial ASL grayscale and color CBF maps (**F, G**)

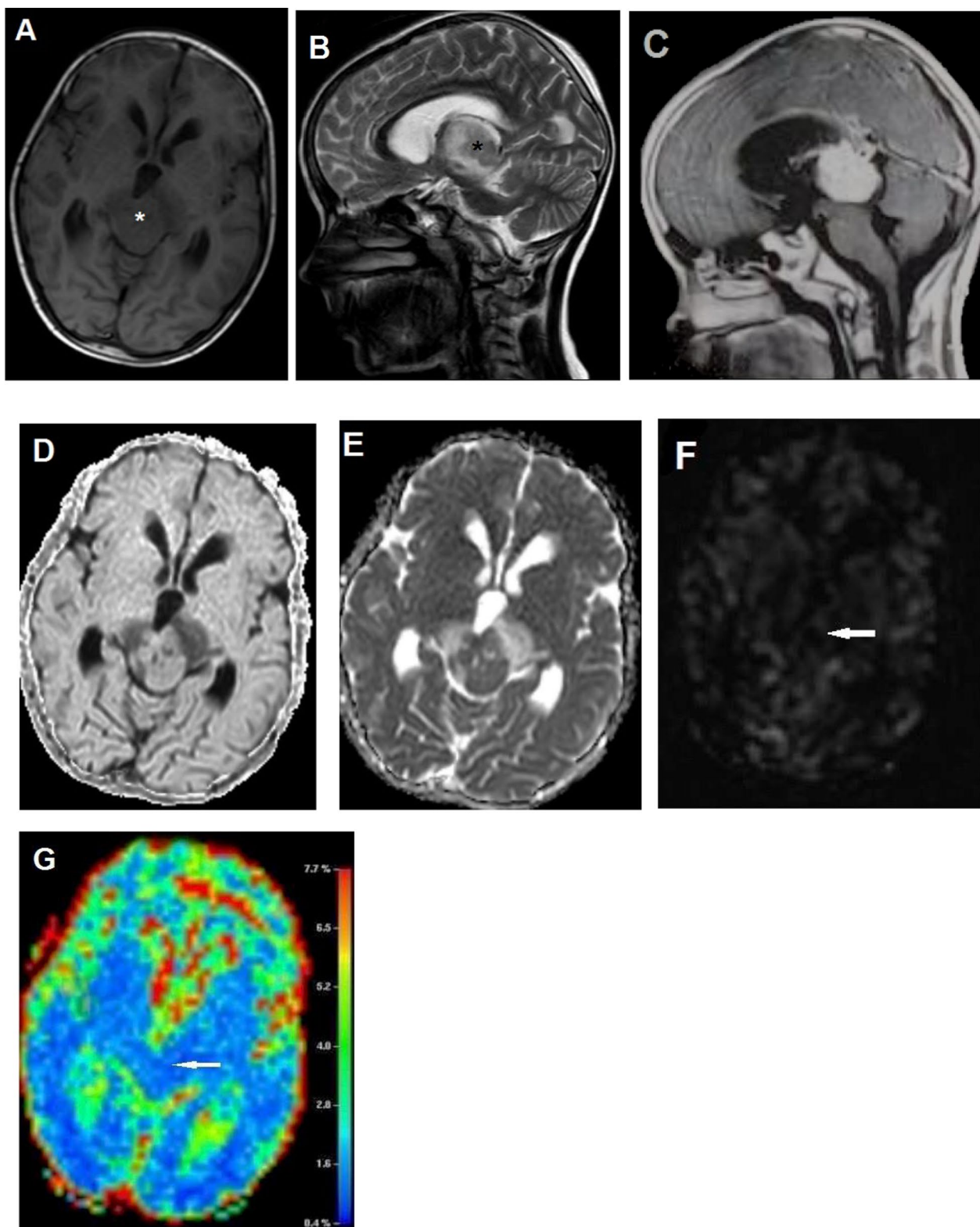


Fig. 3 A 10-year-old boy patient with a WHO grade 2 pineal body tumor of intermediate differentiation. Images show a well-defined pineal body lesion with supra-tentorial hydrocephalic changes. It displays low signal intensity on axial T1WI (**A**) and intermediate to high SI with high SI perilesional edema on sagittal T2WI (**B**). It shows strong homogenous enhancement on post contrast sagittal T1WI (**C**), the lesion shows free diffusion as shown on both DWI (b1000 image) and axial ADC grayscale map (**D,E**). Hypo-perfusion of the lesion (white arrows) is demonstrated in the axial ASL grayscale and color CBF maps (**F, G**)

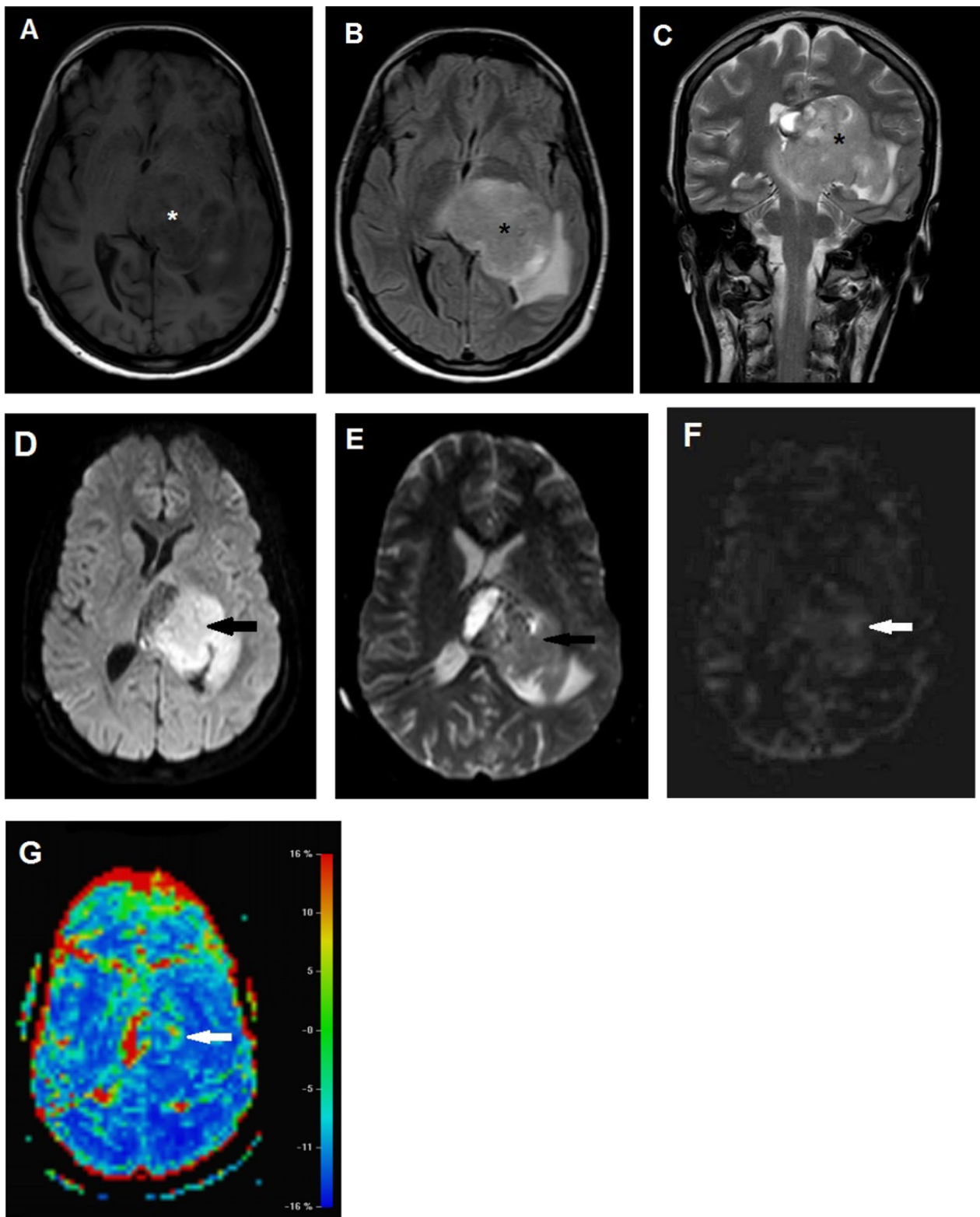


Fig. 4 A 16-year-old girl patient with a WHO grade IV glioma; images show a large mass of non-homogeneous signal intensity in the left thalamic and deep periventricular white matter (asterisk). It displays low SI on axial T1WI (A), high SI on axial FLAIR image (B). It is seen crossing midline with associated high T2SI edema and mass effect in coronal T2-weighted image (C). It shows restricted diffusion (black arrows) in the form of high SI on DWI (b1000 image) and low SI on ADC grayscale map (E, D). High perfusion of the mass (white arrows) is seen in axial ASL grayscale and color CBF maps (F, G)

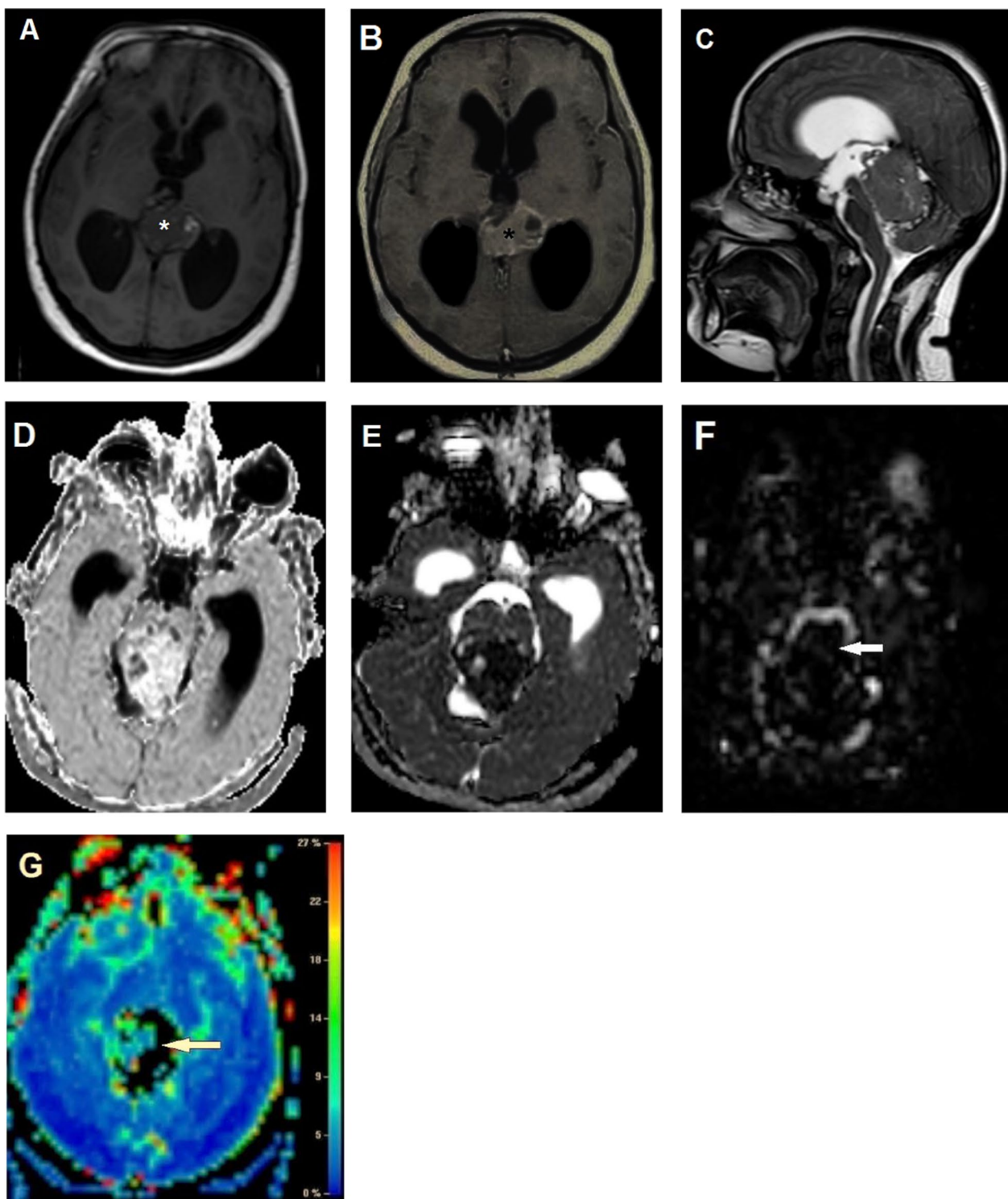


Fig. 5 A 15-year-old girl patient with WHO grade 4 medulloblastoma. Images show a fourth ventricular mass of non-homogenous signal intensity (asterisk) displaying low SI with hemorrhagic foci of high SI on axial T1WI (A) with heterogeneous enhancement on post contrast axial T1WI (B). Its origin from the roof of fourth ventricle can be demonstrated in sagittal T2WI (C). It shows restricted diffusion in the form of high SI on DWI (b1000 image) and low SI on axial ADC grayscale map (D, E). There is mixed perfusion of the lesion (white arrows) on Axial ASL grayscale and color CBF maps (F, G)

Table 1 Site of the studied lesions

Site	n = 32	%
Cerebral hemispheres	8	25.0
Posterior fossa	12	37.5
Sellar/suprasellar	4	12.5
Intraventricular	2	6.25
Pineal	2	6.25
Brain stem / thalamus	4	12.5

Our study aimed to emphasize the role of ASL perfusion MRI in the prediction of the grading of pediatric brain tumors which may help in the management and follow-up of those patients. Many studies have discussed the role of perfusion studies in adult brain tumors. However, not as many studies have been conducted on pediatric brain tumors which have unique features different from adult tumors [22, 23]. Most of these studies have largely concentrated on dynamic susceptibility contrast (DSC) perfusion imaging, the most widely used technique for assessing brain tumor perfusion [24].

This study included 32 patients in the pediatric age group (less than 18 years old). The patients were grouped according to the pathological findings into low-grade tumors (including WHO grades I and II, including 23 patients: 18 patients with grade I and 5 patients with grade II) and high-grade tumors (including WHO grades III and IV, including 9 patients: 1 patient with grade III and 8 patients with grade IV). All lesions in the current study had histopathologically proven diagnoses.

In our study, quantification of absolute tumor blood flow (aTBF) was done by placing ROIs manually by both observers within the high signal area on the ASL grayscale map, avoiding the regions of vessels, calcification, hemorrhage, cystic, and necrotic areas. The values obtained from both observers were analyzed and compared, and there was an excellent inter-observer agreement (ICC = 0.978).

A previous study had found that aCBF values varied between both observers as the CBF_{max} must be normalized to normal-appearing gray matter, the measurement of which is subject to fluctuation between readers. It is difficult and subjective for a reader to identify the maximum CBF location of a tumor “by eye.” However, they

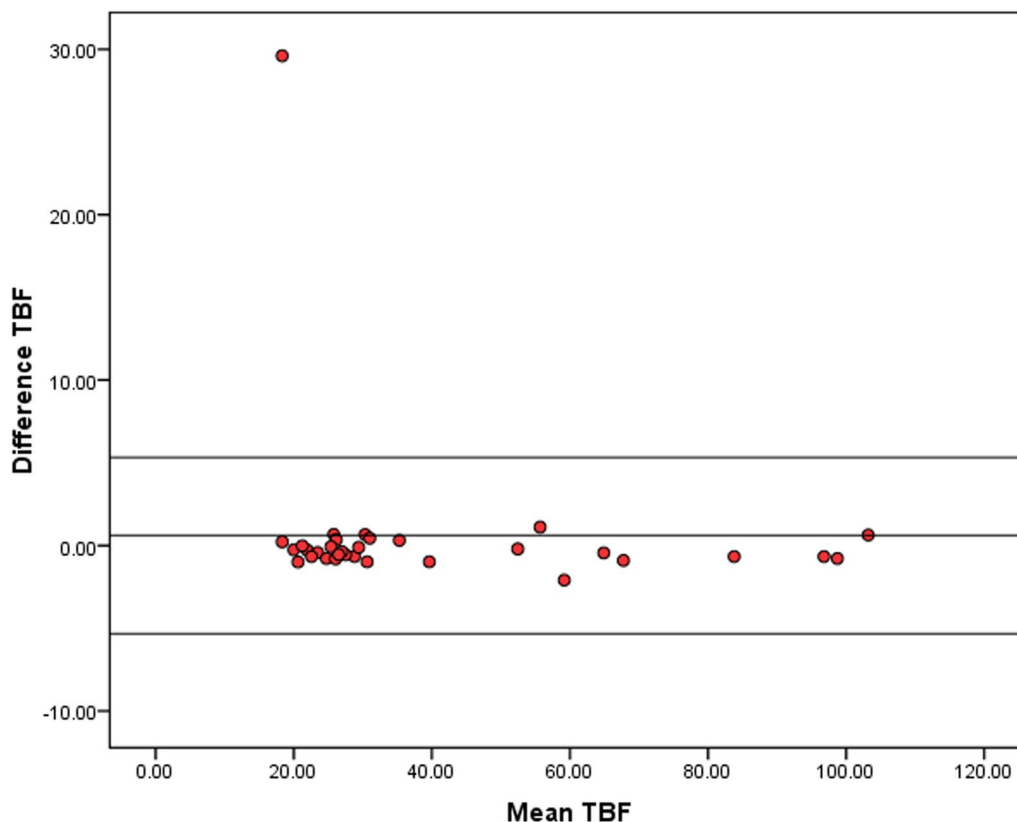


Fig. 6 Bland-altman analysis for agreement between first and second observers as regard aTBF

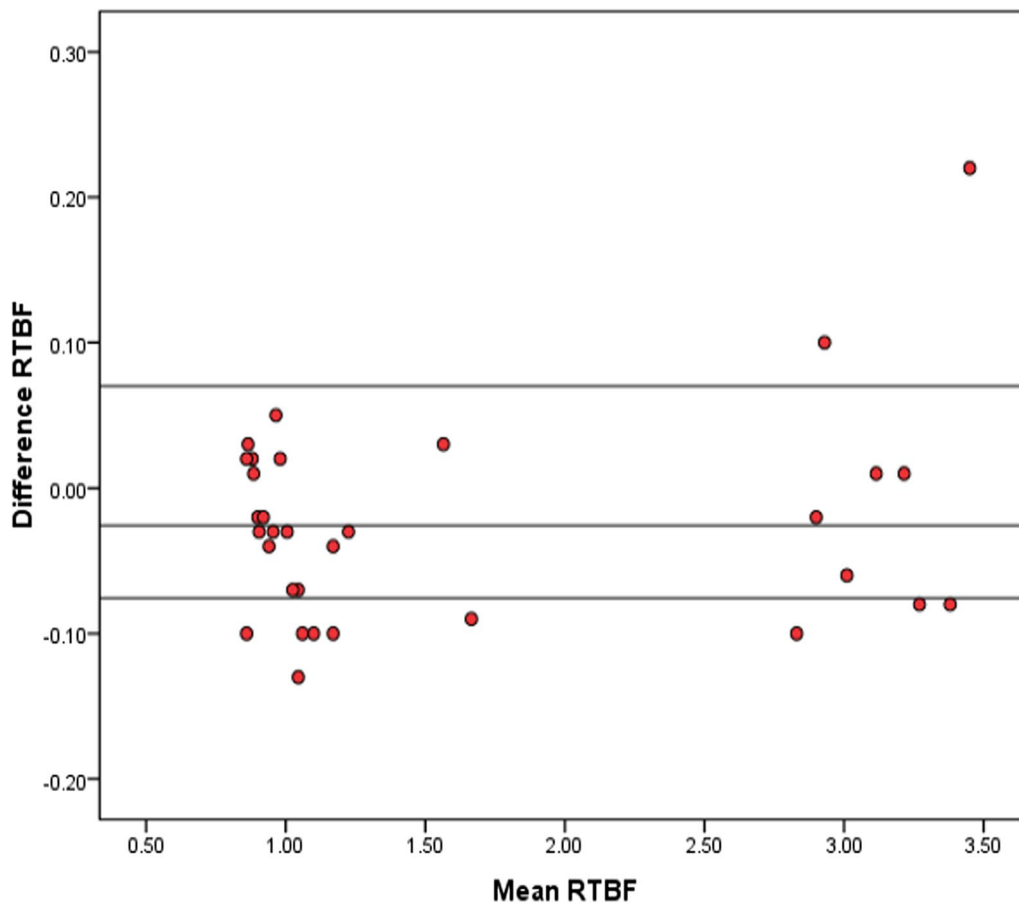


Fig. 7 Bland-altman analysis for agreement between first and second observers as regard rTBF

Table 2 Agreement between first and second observers as regard absolute and relative TBF (ICC: inter-class correlation coefficient)

	First observer	Second observer	ICC (95% CI)
Absolute TBF	28.9 (18.45–103.52)	28.45 (3.51–102.88)	0.978 (0.955–0.989)
Relative TBF	1.01 (0.81–3.56)	1.11 (0.85–3.42)	0.997 (0.997–0.999)

stated that for readers 1 and 2, personally measured values yielded low-/high-grade prediction accuracy of 92% and 96%, respectively. Therefore, it does not seem that the low precision and accuracy of manually measured data significantly reduce their diagnostic relevance, and their use is justified in the absence of automated tumor sampling techniques [25].

Table 3 Inter-observer agreement as regard qualitative assessment of the studied lesions

Qualitative assessment	First observer N= 32	Second observer N= 32	Kappa agreement (95% CI)	SE of kappa	% of agreement
Hypo-perfused	20	18	0.779	0.098	87.0%
Hyper-perfused	7	7	(0.587–0.972)		
Mixed	5	7			

Table 4 Mean absolute and relative TBF according to WHO grade of the studied lesions

	Grade 1	Grade 2	Grade 3&4	Test of significance
Absolute TBF	24.64 ± 3.45 ^A	33.81 ± 3.59 ^B	75.60 ± 20.0 ^{AB}	F = 66.44 P < 0.001*
Relative TBF	1.01 ± 0.17 ^A	1.07 ± 0.31 ^B	3.12 ± 0.24 ^{AB}	F = 298.80 P < 0.001*

* statistically significant

Similar superscripted letters in same row denote significant difference between groups

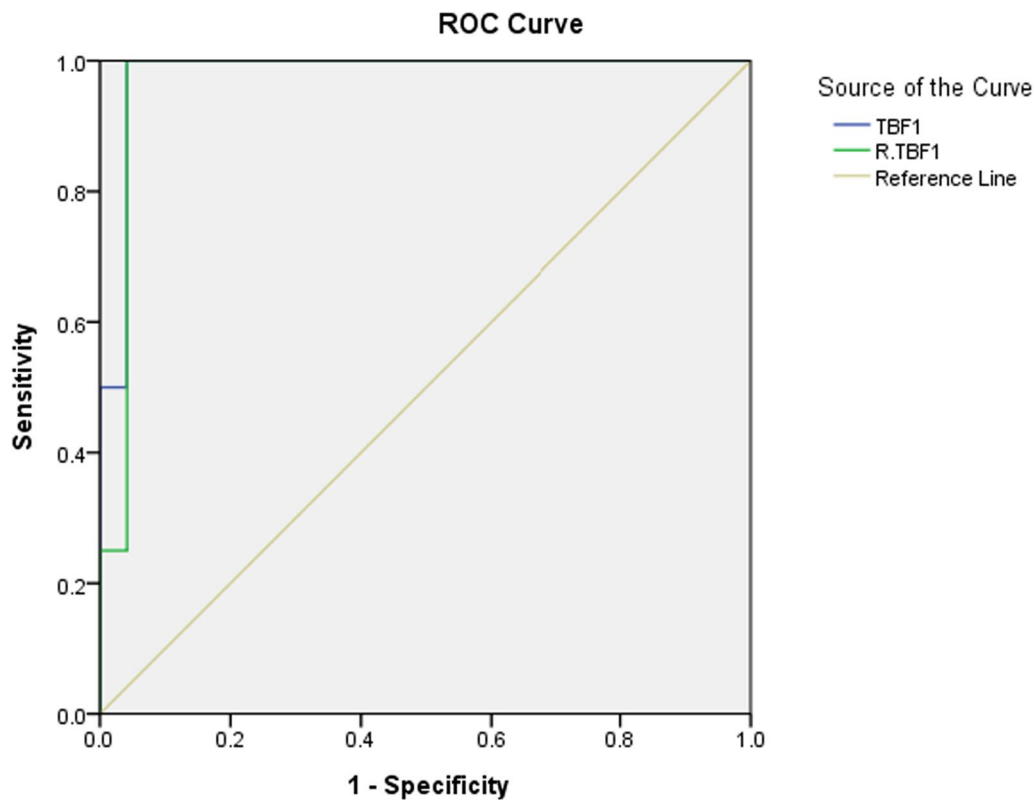


Fig. 8 ROC curve of aTBF and rTBF in differentiating low from high grade

Table 5 ROC curve of TBF, RTBF in differentiating low- from high-grade tumors (AUC: area under curve, PPV: Positive predictive value, NPV: Negative predictive value)

	AUC (95% CI)	P value	Cut off point	Sensitivity%	Specificity%	PPV%	NPV%	Accuracy%
aTBF	0.979 (0.934–1.0)	< 0.001*	54.29	87.5	95.8	87.5	95.8	93.8
rTBF	0.969 (0.906–1.03)	< 0.001*	2.84	87.5	95.8	87.5	95.8	93.8

* statistically significant

There was also excellent agreement between both observers in the assessment of relative tumor blood flow by obtaining the ratio between the ROI placed by both observers in the tumor region and the other ROI placed in the contralateral normal gray matter.

Another study instead preferred placing the other ROI in the contralateral healthy brain tissue, which contains

white matter, gray matter, and vascular structures, to calculate the average mean signal intensity of the size-matched contralateral normal brain tissue (normal ROI). This normalization was applied to remove signals from normal vascular and parenchymal structures [26].

On the other side, normal appearing white matter has a long transit time and a higher water content in the case of

brain tumors, so that some researches claim that utilizing white matter as a reference ROI is still debatable. This, in turn, could lead to an underestimation of white matter CBF value by ASL [27].

A study was done by Testud et al. [28] on the role of both dynamic susceptibility contrast (DSC) and ASL MRI perfusion, which concluded that low- and high-grade pediatric brain tumors can be distinguished with DSC and ASL perfusion techniques; however, the accuracy is location- and field-dependent. For supra-tentorial malignancies, DSC outperforms ASL with excellent results, while in posterior fossa lesions, ASL seems to function more effectively.

Arterial spin-labeled perfusion study enabled us to predict tumor grades in studied cases by quantitative assessment of absolute and relative tumoral flow. Compared to low-grade tumors, values were higher in high-grade tumors. In ROC analysis, the AUC of absolute and relative TBF to differentiate low- from high-grade tumors was (0.979 and 0.969, respectively). The calculated cutoff points to discriminate between high- and low-grade tumors were (54.29 ml/100 g/min) for aTBF and (2.84) for rTBF which revealed accuracy of (93.8%), sensitivity of (87.5%), specificity of (95.8%), PPV of (87.5%), and NPV of (95.8%).

In keeping with our results, other studies were done using ASL techniques for differentiating high- (III, IV) from low-grade (I, II) tumors revealing higher CBF in high- than low-grade brain tumors with a high significant difference [29, 30].

A similar study was conducted by Morana et al. [31] on 37 children with pathologically proven astrocytomas of different tumor grades, in which ROC analysis demonstrated the AUC of rTBF to differentiate low- from high-grade astrocytomas was 0.96, which showed a significant correlation with DSC calculated values.

Another study done by Dangouloff-Ros et al. [32] on 129 children with brain tumors demonstrated that the cutoff points of aTBF and rTBF were (50 mL/min/100 g) and (0.95), respectively, to distinguish low- from high-grade tumors.

We found, in keeping with previous studies, that ASL-weighted perfusion maps and CBF maps are really useful for investigating, evaluating, and quantifying brain tumors in pediatrics. They have many advantages, such as the limitation of the irradiation dose to some vulnerable tissues and organs in children. Additionally, there is no contrast medium that permits intraoperative imaging of pediatric brain tumors as well as repetition of the study for follow-up [33, 34].

Limitations

There were some limitations in our study, which we can conclude in a few points. First, the current study enrolled a small number of patients in a single center,

which has limited the statistical results. It is advised to do future research with a larger number of patients who have a variety of pathological findings and to conduct multicenter studies. Second, our study was conducted using a 1.5 Tesla MR machine, so we faced a problem of low SNR and motion artifacts in some cases. Further studies using 3 Tesla MR machines may help improve the results. Third, as regards the grading of brain tumors we depended on measuring TBF. Further studies with the application of diffusion tensor imaging and proton MR spectroscopy, as well as molecular and genetic tumor classification, will improve the prediction of pediatric brain tumors grades.

Conclusions

It was found that high-grade tumors have higher absolute and relative TBF than low-grade tumors. Therefore, MR imaging with ASL can be used to classify pediatric brain tumors relying on TBF. The relationship between ASL and WHO tumor grade adds further insight into the understanding of pediatric brain tumors.

Arterial spin labeling is a noninvasive, promising, and recent perfusion imaging technique that offers some merits. Firstly, it does not require the use of an exogenous contrast agent, which is beneficial in the pediatric population. Secondly, it is also a fast and repeatable technique, which is an advantage in the follow-up of those patients throughout their treatment journey. Finally, it may produce results that would be a helpful alternative technique for assessment of brain tumors perfusion, predicting its grade and guiding histopathological sampling in those patients. Hence, we recommend that it be included in the routine MRI protocol.

Abbreviations

ASL	Arterial spin labeled
MRI	Magnetic resonance imaging
aTBF	Absolute tumoral blood flow
rTBF	Relative tumoral blood flow
CNS	Central nervous system
T1WI	T1-Weighted image
T2WI	T2-Weighted image
FLAIR	Fluid-attenuated inversion recovery
DWI	Diffusion-weighted imaging
TR	Repetition time
TE	Echo time
Ti	Inversion time
FOV	Field of view
SOLs	Space occupying lesions
ROIs	Regions of interest
CBF	Cerebral blood flow
ICC	Inter-class correlation coefficient
AUC	Area under the curve
PPV	Positive predictive value
NPV	Negative predictive value
DSC	Dynamic susceptibility contrast

Acknowledgements

Not applicable.

Author contributions

All authors read and approved the final manuscript.

Funding

No funding supported this research.

Availability of data and materials

The datasets used and/or analyzed during the current study are available from the corresponding author on reasonable request.

Declarations**Ethics approval and consent to participate**

The study was approved by our institution's ethics committee (Mansoura Faculty of Medicine Institutional Research Board) (ethics committee reference number is MD.20.03.299). A verbal informed consent was obtained from all patients (their parents) included in the study.

Consent for publication

Not applicable.

Competing interests

The authors declare that they have no competing interests.

Received: 10 May 2023 Accepted: 30 July 2023

Published online: 08 August 2023

References

- Malbari F, Lindsay H (2020) Genetics of common pediatric brain tumors. *Pediatr Neurol* 104:3–12
- Ostrom QT, Cioffi G, Gittleman H, Patil N, Waite K, Kruchko C, Barnholtz-Sloan JS (2019) CBRUS statistical report: primary brain and other central nervous system tumors diagnosed in the United States in 2012–2016. *Neuro Oncol* 21(5):1–100
- Udaka YT, Packer RJ (2018) Pediatric brain tumors. *Neurol Clin* 36(3):533–556
- Spennato P, Nicosia G, Quaglietta L, Donofrio V, Miron G, Di Martino G, Cinalli G (2015) Posterior fossa tumors in infants and neonates. *Childs Nerv Syst* 31:1751–1772
- Fischer C, Petriccione M, Donzelli M, Pottenger E (2016) Improving care in pediatric neuro-oncology patients: an overview of the unique needs of children with brain tumors. *J Child Neurol* 31(4):488–505
- Chu TP, Shah A, Walker D, Coleman MP (2015) Pattern of symptoms and signs of primary intracranial tumours in children and young adults: a record linkage study. *Arch Dis Child* 100(12):1115–1122
- Scala M, Fiaschi P, Cama A, Consales A, Piatelli G, Giannelli F, Pavanello M (2020) Radiation-induced moyamoya syndrome in children with brain tumors: case series and literature review. *World Neurosurg* 135:118–129
- Pandhi A, Krishnan R, Goyal N, Malkoff M (2020) Increased intracranial pressure in critically ill cancer patients. *Oncol Crit Care* 8:395–407
- Smits M (2021) MRI biomarkers in neuro-oncology. *Nat Rev Neurol* 17(8):486–500
- Han H, Han C, Wu X, Zhong S, Zhuang X, Tan G, Wu H (2017) Preoperative grading of supratentorial nonenhancing gliomas by high b-value diffusion-weighted 3 T magnetic resonance imaging. *J Neurooncol* 133:147–154
- Borja MJ, Plaza MJ, Altman N, Saigal G (2013) Conventional and advanced MRI features of pediatric intracranial tumors: supratentorial tumors. *Am J Roentgenol* 200(5):W483–W503
- Caravan I, Ciortea CA, Contis A, Lebovici A (2018) Diagnostic value of apparent diffusion coefficient in differentiating between high-grade gliomas and brain metastases. *Acta Radiol* 59(5):599–605
- Nery F, Gordon I, Thomas DL (2018) Non-invasive renal perfusion imaging using arterial spin labeling MRI: challenges and opportunities. *Diagnostics* 8(1):2
- Khanal S, Turnbull PR, Vaghefi E, Phillips JR (2019) Repeatability of arterial spin labeling MRI in measuring blood perfusion in the human eye. *J Magn Reson Imaging* 49(4):966–974
- Odudu A, Nery F, Hartevelde AA, Evans RG, Pendse D, Buchanan CE, Fernández-Seara MA (2018) Arterial spin labelling MRI to measure renal perfusion: a systematic review and statement paper. *Nephrol Dial Transplant* 33(2):15–21
- Ludwig KD, Fain SB, Nguyen SM, Golos TG, Reeder SB, Bird IM, Johnson KM (2019) Perfusion of the placenta assessed using arterial spin labeling and ferumoxylol dynamic contrast enhanced magnetic resonance imaging in the rhesus macaque. *Magn Reson Med* 81(3):1964–1978
- Conlin CC (2019) Functional assessment of the kidneys with magnetic resonance imaging and tracer-kinetic modeling. Doctoral dissertation, The University of Utah
- Francis S (2020) Arterial spin labeling MRI: basic physics, pulse sequences, and modeling. In: *Advances in magnetic resonance technology and applications*, vol 1. Academic Press, pp 295–320
- Deibler AR, Pollock JM, Kraft RA, Tan H, Burdette JH, Maldjian JA (2008) Arterial spin-labeling in routine clinical practice, part 1: technique and artifacts. *Am J Neuroradiol* 29(7):1228–1234
- Zhao J, Yang ZY, Luo BN, Yang JY, Chu JP (2015) Quantitative evaluation of diffusion and dynamic contrast-enhanced MR in tumor parenchyma and peritumoral area for distinction of brain tumors. *PLoS ONE* 10(9):e0138573
- Munir S, Khan SA, Hanif H, Khan M (2021) Diagnostic accuracy of magnetic resonance imaging in detection of intra-axial gliomas. *Pakistan J Med Sci* 37(1):125
- Yeom KW, Mitchell LA, Lober RM, Barnes PD, Vogel H, Fisher PG, Edwards MS (2014) Arterial spin-labeled perfusion of pediatric brain tumors. *Am J Neuroradiol* 35(2):395–401
- Shaari H, Kevrić J, Jukić S, Bešić L, Jokić D, Ahmed N, Rajs V (2021) Deep learning-based studies on pediatric brain tumors imaging: narrative review of techniques and challenges. *Brain Sci* 11(6):716
- Ho CY, Cardinal JS, Kamer AP, Kralik SF (2015) Relative cerebral blood volume from dynamic susceptibility contrast perfusion in the grading of pediatric primary brain tumors. *Neuroradiology* 57:299–306
- Hales PW, d'Arco F, Cooper J, Pfeuffer J, Hargrave D, Mankad K, Clark C (2019) Arterial spin labelling and diffusion-weighted imaging in paediatric brain tumours. *NeuroImage Clin* 22:101696
- Furtner J, Schöpf V, Schewzow K, Kasprian G, Weber M, Woitek R, Prayer D (2014) Arterial spin-labeling assessment of normalized vascular intratumoral signal intensity as a predictor of histologic grade of astrocytic neoplasms. *Am J Neuroradiol* 35(3):482–489
- Soni N, Dhanota DPS, Kumar S, Jaiswal AK, Srivastava AK (2017) Perfusion MR imaging of enhancing brain tumors: comparison of arterial spin labeling technique with dynamic susceptibility contrast technique. *Neurol India* 65(5):1046
- Testud B, Brun G, Varoquaux A, Hak JF, Appay R, Le Troter A, Stellmann JP (2021) Perfusion-weighted techniques in MRI grading of pediatric cerebral tumors: efficiency of dynamic susceptibility contrast and arterial spin labeling. *Neuroradiology* 63:1353–1366
- Kong L, Chen H, Yang Y, Chen L (2017) A meta-analysis of arterial spin labelling perfusion values for the prediction of glioma grade. *Clin Radiol* 72(3):255–261
- Yang S, Zhao B, Wang G, Xiang J, Xu S, Liu Y, Qian T (2016) Improving the grading accuracy of astrocytic neoplasms noninvasively by combining timing information with cerebral blood flow: a multi-T1 arterial spin-labeling MR Imaging study. *Am J Neuroradiol* 37(12):2209–2216
- Morana G, Tortora D, Staglianò S, Nozza P, Mascelli S, Severino M, Rossi A (2018) Pediatric astrocytic tumor grading: comparison between arterial spin labeling and dynamic susceptibility contrast MRI perfusion. *Neuroradiology* 60:437–446
- Dangoulouff-Ros V, Deroulers C, Foissac F, Badoual M, Shotar E, Grévent D, Boddaert N (2016) Arterial spin labeling to predict brain tumor grading in children: correlations between histopathologic vascular density and perfusion MR imaging. *Radiology* 281(2):553–566
- Baudou E, Pariette J, Péran P, Tensaouti F, Pollidorio L, Meline D, Laprie A (2022) A prospective behavioral and imaging study exploring the impact on long-term memory of radiotherapy delivered for a brain tumor in childhood and adolescence. *Clin Transl Radiat Oncol* 33:7–14

34. Lindner T, Ahmeti H, Lübbling I, Helle M, Jansen O, Synowitz M, Ulmer S (2017) Intraoperative resection control using arterial spin labeling—proof of concept, reproducibility of data and initial results. *NeuroImage Clin* 15:136–142

Publisher's Note

Springer Nature remains neutral with regard to jurisdictional claims in published maps and institutional affiliations.

Submit your manuscript to a SpringerOpen[®] journal and benefit from:

- ▶ Convenient online submission
- ▶ Rigorous peer review
- ▶ Open access: articles freely available online
- ▶ High visibility within the field
- ▶ Retaining the copyright to your article

Submit your next manuscript at ▶ [springeropen.com](https://www.springeropen.com)
